

Doppler Imaging of Stars with Surface Inhomogeneities

Andrew Collier Cameron

*School of Physics and Astronomy, University of St Andrews, North
Haugh, St Andrews, Fife, SCOTLAND KY16 9SS*

Abstract. I review recent progress in the field of stellar surface imaging, with particular reference to advanced methods for mapping surface-brightness distributions on magnetically active late-type stars. New signal enhancement techniques, utilising profile information from hundreds or thousands of photospheric lines simultaneously, allow images to be derived for stars several magnitudes fainter than was previously possible. For brighter stars, the same techniques make it possible to map features as small as two or three degrees in extent on the stellar surface. While this opens up whole new areas of research, such as the ability to use starspot tracking to study surface differential rotation patterns on single and binary stars, caution must be exercised in the treatment of “nuisance” parameters such as the stellar rotation rate, surface abundances and radial velocity. At the very high S:N levels we now use, the effects of systematic errors in these parameters are easier to identify, isolate and eliminate. This leads to the possibility of making precise radial velocity variations (at the few hundred m s^{-2} level or better) in late-type stars even with equatorial rotation speeds as high as 100 km s^{-1} . This is particularly topical given the recent discovery that one of our prime imaging targets, the young southern K0 dwarf AB Doradus, has an astrometric companion in a highly eccentric orbit with an inferred mass close to the H-burning limit.

1. Introduction

One of the main limitations to precise radial-velocity determinations for young solar-type stars is their extreme rotation and consequently high levels of magnetic activity. Saar, Butler, & Marcy (1998) have found a systematic trend even among moderately slow rotators, for spurious, short-term radial velocity variations to increase systematically with increasing levels of surface magnetic activity. The reason for this is twofold. First, the rotational Doppler effect tends to blur the line profiles, decreasing the first derivative of the profile at its steepest part, thereby decreasing the precision with which line shifts can be measured. Secondly, it is now well established that magnetic activity levels, and in particular the surface covering fraction of dark starspots, increases in more or less direct proportion to rotation rate in stars of a given spectral type. The presence of starspots in a rotationally broadened line profile leads to periodic distortion of the profile shape. Elsewhere in these proceedings, Hatzes

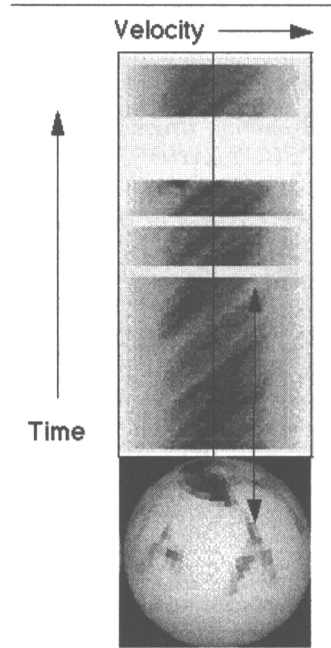


Figure 1. Schematic illustration of the basic principles of Doppler imaging for spotted stars. The spectral signature of the light “missing” from the spotted regions contains a Doppler-shifted absorption line, leaving bright bumps in the observed spectrum which migrate across the stellar disk at a rate that depends on the spot’s stellar latitude.

demonstrates how spurious velocity variations arising from a given spot configuration should increase more or less linearly with $v \sin i$. In reality, things are even worse. Since spot coverage increases linearly with rotation rate, we expect the amplitude of the spurious velocity variations to scale more as the square of $v \sin i$. In this review, I give an account of recent developments in the study of stellar surface features *per se*. Following on from this, I discuss the possibilities for using imaging techniques to model the profile distortions imposed by surface activity, and investigate the limiting precision on the radial velocity measurements that should be possible in the not-too-distant future even for very young, rapidly rotating late-type stars.

2. General principles

The main requirement for successful Doppler imaging is that the rotational Doppler effect should be the dominant line broadening mechanism for the majority of photospheric absorption lines. Each surface element on the star contributes

a limb-darkened and Doppler-shifted copy of the local specific intensity profile. Integration over the visible disk at any instant then gives the rotationally-broadened spectrum. A dark spot on the stellar surface can then be regarded as a region where there is a deficit in the local spectrum. This has the effect of depressing the continuum slightly at all wavelengths, and leaving bright but narrow “bumps” in the photospheric absorption-line profiles. For the case of solid-body rotation, the displacement of the bump from line centre is directly proportional to the projected distance of the spot from the stellar rotation axis. A sequence of spectra (Fig. 1) then shows these bumps drifting across the profile at rates dictated by the latitudes of the spots in which they originate.

Vogt & Penrod (1983) used this phenomenon to pin down (by trial and error) the locations of spots on the surface of the subgiant component of HR 1099. Given a map of the spots on the stellar surface, and a physical model for the specific intensity spectrum of radiation emerging from the spotted and unspotted regions on the stellar surface, it is relatively straightforward to predict the form of the observed spectral-line profiles at any given rotation phase. The stellar image is treated as a vector of dimension M , containing either local temperatures or spot filling factors, on a grid of pixels with pre-determined locations and surface areas. The observations can also be treated as a vector of dimension N , containing the spectral fluxes observed at each wavelength in a succession of spectra spanning the rotation cycle. The functional dependence of the local specific intensity on the local image pixel value and foreshortening angle at each observed rotation phase is encoded in the elements of a $M \times N$ transformation matrix. The forward transformation of the image values into a synthetic data set is effected by computing the product of the transformation matrix with the image vector.

Vogt, Penrod, & Hatzes (1987) refined the technique further by applying the Maximum Entropy Method of Skilling & Bryan (1984) to the problem of recovering an image that was unique in the sense of determining the “simplest” image capable of yielding a satisfactory fit to the data. Several other groups developed Doppler imaging codes within the next few years, and achieved broadly similar results. The misfit between the resulting synthetic data and the observations is usually quantified by χ^2 or an equivalent statistic. A regularising function such as the image entropy (see, e.g. Brown et al. 1991, Collier Cameron 1992, Piskunov & Rice 1993) or the Tikhonov smoothness criterion (Rice, Wehlau, & Khokhlova 1989, Piskunov, Tuominen, & Vilhu 1990) may also be computed, if the data are sparse or noisy enough for the problem to be ill-conditioned. The image is then improved iteratively using a search algorithm based on the image-space gradients of both the fitting statistic and the regularising function. Other approaches to the iterative improvement of the image include Kürster’s (1993) CLEAN-like algorithm, and the occamian approach of Berdyugina, Ilyin, & Tuominen (1998), which is essentially an adaptation of singular-value decomposition. In all these methods, the reconstruction is halted once a satisfactory fit to the data has been achieved (at an extremum of the regularising function, if appropriate).

3. Least-squares deconvolution

Extreme rotation has the effect of making the photospheric absorption lines extremely broad and shallow. The amplitudes of the bumps produced by starspots are reduced accordingly, and in spectra with low signal-to-noise (S/N) ratios, faint spot features may be deeply buried in noise. Donati et al. (1997) overcame this problem through the use of a technique known as *least-squares deconvolution*, which extracts averaged profile information from the thousands of photospheric lines that are recorded in a typical echelle spectrum.

The method works by treating the observed spectrum r as the convolution f of a “mean” line profile z with a set of weighted delta functions at the wavelengths of a comprehensive list of spectral lines. This operation can be written in matrix form as

$$\mathbf{f} = \mathbf{A} \cdot \mathbf{z} \quad (1)$$

The line weights, incorporated in the convolution matrix \mathbf{A} , are proportional to the central depths of the lines as computed from a Kurucz model atmosphere for the appropriate spectral type. The elements α_{jk} of the matrix \mathbf{A} are computed by summing over all spectral lines i , the fractional contribution to data pixel j of the k th element of the profile when the centre of the deconvolved profile is shifted to the wavelength λ_i of each line in turn. The profile is normally defined on a linear velocity scale, with a velocity increment comparable to the average pixel velocity increment in the data.

The mean profile is then recovered from the observed spectrum and the convolution matrix by the method of least squares. This entails solving the matrix equation

$$\mathbf{A}^T \cdot \mathbf{V} \cdot \mathbf{A} \cdot \mathbf{z} = \mathbf{A}^T \cdot \mathbf{V} \cdot \mathbf{r}, \quad (2)$$

where the inverse variances σ_j^2 associated with the N elements r_j of the residual spectrum r are incorporated via the diagonal matrix

$$\mathbf{V} = \text{Diag}[1/\sigma_1^2, \dots, 1/\sigma_N^2]. \quad (3)$$

Since the square matrix $\mathbf{A}^T \cdot \mathbf{V} \cdot \mathbf{A}$ is symmetric and positive-definite, the least-squares problem can be solved using efficient methods such as Cholesky decomposition (Press et al. 1992).

In terms of signal improvement, this method is analogous to aligning and co-adding (with appropriate weighting factors for line strength and local continuum signal strength on the recorded frame) the profiles of the 2000 or so images of the 1500-odd individual photospheric absorption lines recorded on each echellogram. The deconvolution procedure compensates for local line blends, and so has the advantage over cross-correlation methods that outside the region occupied by the residual stellar profile, the deconvolved spectrum is flat. The formal errors on the M points of the deconvolved profile are obtained in the usual way from the diagonal elements of the $M \times M$ inverse matrix $\mathbf{C} = [\mathbf{A}^T \cdot \mathbf{V} \cdot \mathbf{A}]^{-1}$.

4. Differential rotation from starspot tracking

Donati & Collier Cameron (1997) and Donati et al. (1999) applied least-squares deconvolution to echelle spectra of the rapidly rotating southern K0 dwarf star

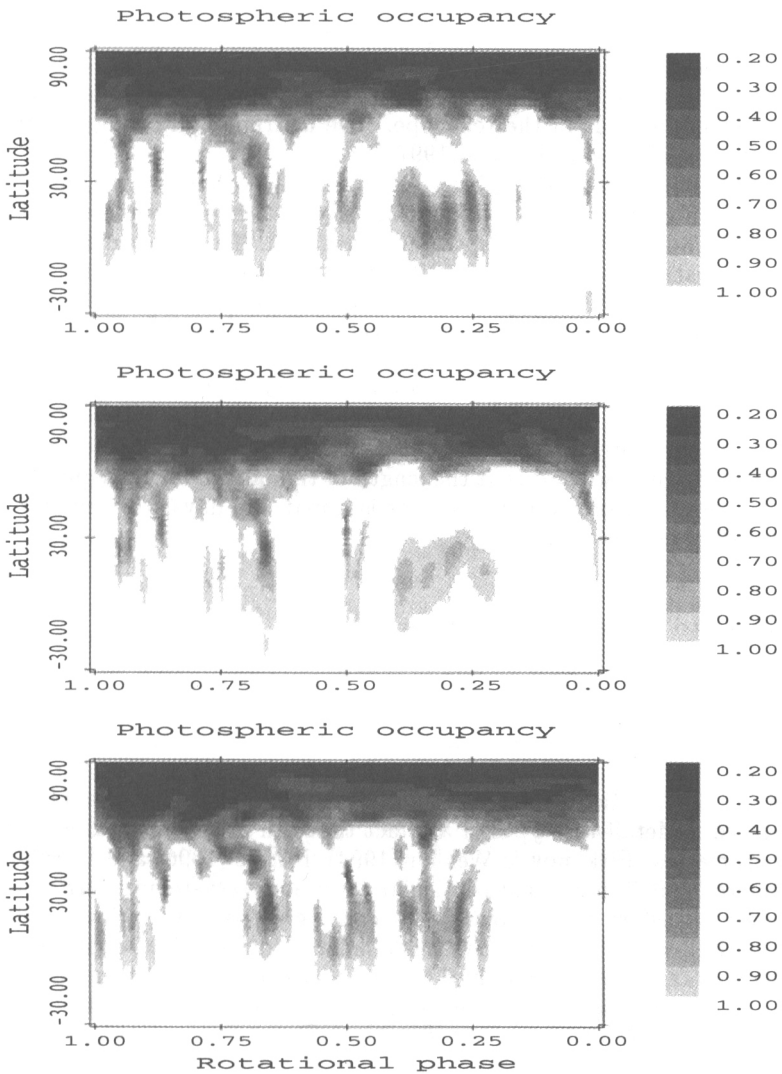


Figure 2. Three maps of the surface brightness distribution on AB Dor, on the nights of 1996 December 23+25 (top), 27 (middle) and 29 (bottom). Note relative phase drift of high- and low-latitude features in the best-observed phase range in the left-hand half of each map. Adapted from Donati et al. (1999).

AB Doradus in 1995 December and 1996 December. The observations were secured with the UCL Echelle Spectrograph (UCLES) on the 3.9-m *Anglo-Australian Telescope*, fed by a dual-fibre circular spectropolarimeter mounted at the cassegrain focus of the telescope. The instrumental configuration is described in detail by Donati et al. (1997).

The deconvolved profiles, based on nearly 2000 line images, have a S/N ratio that is higher by a factor of 30 than any of the relatively few un-blended photospheric lines found in the spectral region used. This allowed us for the first time to reconstruct surface images without having to resort to binning in either wavelength or time. The exquisite detail seen in the resulting images (Fig. 2) allowed us to use individual spots as tracers of the surface differential rotation pattern from the equator to the perimeter of the dark polar spot, at stellar latitude 70° or so. A latitude-by-latitude cross-correlation of images obtained up to 8 nights apart shows clearly that the star's equator rotates faster than its poles. Surprisingly, in spite of the fact that AB Dor rotates some 50 times faster than the Sun, we find that the length of time taken for the equator to pull one full turn ahead of the polar regions is about 120 days, very similar to the corresponding figure for the Sun.

5. Limits to radial-velocity determination

The structure of the reconstructed image is extremely sensitive to "nuisance parameters" such as the radial velocity of the star, the equatorial rotation speed of the star, and the effects of metallicity on the mean equivalent width of the photospheric lines contributing to the reconstruction. Several authors, notably Vogt et al. (1987), Rice et al. (1989) and Unruh & Collier Cameron (1995) have investigated in detail the types of artefact that can arise from bad estimates of these parameters. Piskunov & Wehlau (1994), Hatzes (1996) and Unruh & Collier Cameron (1997) have paid particular attention to systematic errors in their image-data transformation models that could give rise to spurious dark polar features. High-latitude spot activity is almost ubiquitous in Doppler images of active cool stars, and remarkably difficult to explain away as being due to systematic errors. A consensus now seems to be emerging that these polar features are indeed a real phenomenon, significantly different from anything seen on the Sun.

The enhanced S/N of deconvolved line profiles makes it particularly important to monitor carefully the zero point of the instrumental velocity scale. Fig.3 illustrates the magnitude of the first derivative of a typical deconvolved line profile of AB Dor, in relation to the size of the error bars. In order to achieve a satisfactorily low value of χ^2 in terms of photon statistics alone, the shift of the spectrum must be determined to a precision of order 50 m s^{-1} . Failure to correct random instrumental shifts of more than this magnitude can prevent the reconstruction algorithm from converging to a statistically satisfactory solution.

There are other, astrophysical reasons for attempting to improve the precision of radial velocity measures for these young, rapidly rotating objects. Detailed imaging studies of pre-main sequence stars (e.g. Hatzes 1994, Rice & Strassmeier 1996, Unruh, Collier Cameron, & Guenther 1998) show them generally to be magnetically active, rapid rotators, and any attempt to search for

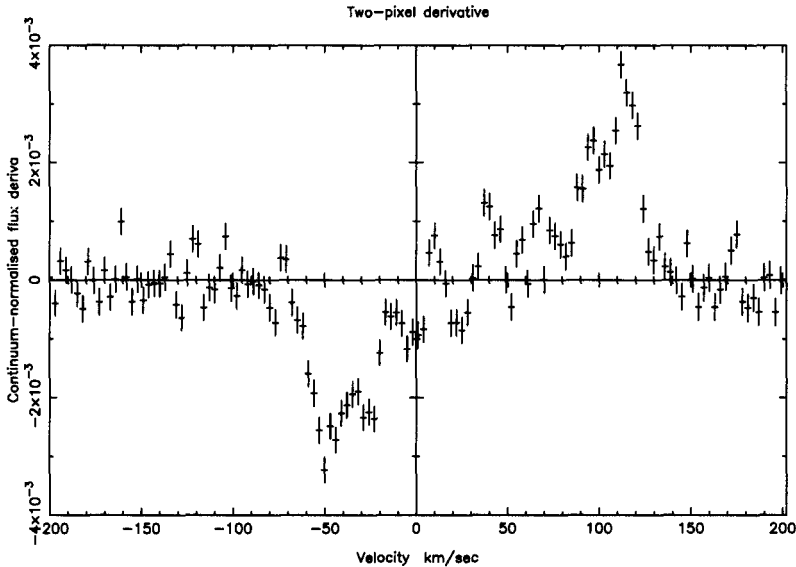


Figure 3. Estimate of first derivative $(f_{j+1} - f_{j-1})/2$ for two-pixel shift of a typical line profile, with photon-limited internal error bars. Subtracting positive and negative residuals on opposite sides of profile gives formal error on radial velocity $\Delta v = 56 \text{ m s}^{-1}$.

planetary and brown-dwarf companions to pre-main sequence stars will require both precise radial velocity measurements and compensation for the effects of surface features. Similar arguments apply to the determination of precise orbital parameters for spotted stars in RS CVn and related binaries when deconvolution is used to obtain high-quality broadening functions, as Donati et al. (1997) have done. Kinematic studies of late-type members of young stellar groups will require radial velocities of a precision commensurate with the best proper-motion estimates available.

As an example, consider the recent discovery by Guirado et al. (1997) of an astrometric companion to AB Doradus. The companion (not to be confused with the common-proper-motion dMe companion Rst 137B) appears to have a mass close to the hydrogen-burning limit, but several more years' observation will be required to tie down the orbital period of the newly-discovered component. The dimensions of the orbit suggest that the reflex motion of AB Dor itself could have an amplitude as great as 2 km s^{-1} or more. This has led us to consider re-analysing our archival imaging data on AB Dor, spanning the period from 1988 December to the present, in an attempt to determine the spectroscopic orbit.

To do this successfully we need to be able to monitor the zero-point of the instrumental velocity in a way that can be applied to archival data, and that can be used in conjunction with the deconvolution technique described above in order to ensure that the deconvolved profiles are placed on a precisely reproducible velocity scale. To this end we have experimented with the inclusion of a list

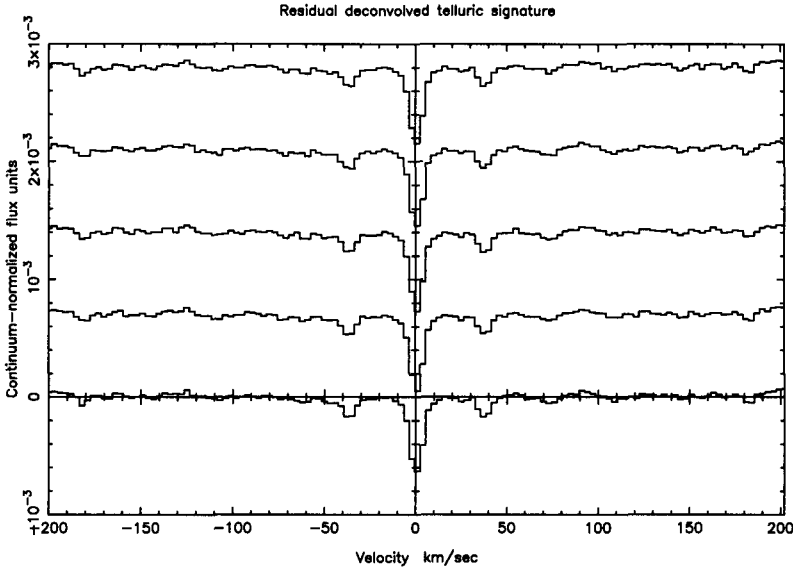


Figure 4. Residual profiles obtained by subtracting profiles deconvolved with a list of stellar lines only, from profiles deconvolved with a list of stellar plus telluric lines. Shifts (bottom to top, relative to the first in this sequence of five spectra) are 0, 94.7, 113.2, -3.4 and 61.89 m s^{-1} .

of telluric lines, drawn from the solar line list of Moore, Minnaert, & Houtgast (1966), in the line list used for the deconvolution itself.

The result is at first glance hardly distinguishable from the profile deconvolved using the stellar line list alone. The difference between the two profiles, however, contains a strong residual signature near zero instrumental velocity (Fig. 4). The RMS scatter in the value of any given pixel in the five sequential observation shown in Fig. 4 is close to 6.6×10^{-6} times the continuum level. The main telluric dip has a depth some 100 times greater than this level, which suggests that the peak position can be determined to an RMS precision of about 50 m s^{-1} . Cross-correlation of the residual spectra confirms that the RMS scatter in the actual values is 54 m s^{-1} , consistent with this estimate.

6. Summary and future prospects

The use of least-squares deconvolution to determine high-quality broadening functions for rapidly rotating stars has led to a significant improvement in our ability to discern fine detail on the surfaces of rapidly rotating stars. In particular, it now allows us to use starspots as tracers of the surface differential rotation patterns on stars other than the Sun. Although at the time of writing this has been achieved for only one star, AB Dor, further observations are scheduled in the next few months to secure differential rotation measurements for a further

six or seven stars with half-day rotation periods and spectral types ranging from early G to early M.

We also conclude that the prospects are good for obtaining precise radial velocity measurements from archival Doppler imaging data on rapidly rotating stars. Least-squares deconvolution not only allows us to map stellar surfaces in unprecedented detail, but can also be adapted to allow monitoring of the instrumental zero point using telluric absorption signatures. This method appears to be capable of providing the 50 m s^{-1} precision demanded by the S:N levels of the deconvolved profiles. It also opens up the possibility of measuring the spectroscopic orbits of low-mass companions to rapidly rotating, active pre-main sequence stars.

References

- Berdyugina, S.V., Ilyin, I., & Tuominen, I. 1998, in *Cool Stars, Stellar Systems, and the Sun* (ASP Conf. Ser., 154), R.A. Donahue & J.A. Bookbinder, San Francisco: Astron. Soc. Pacific, 1952
- Brown, S.F., Donati, J.-F., Rees, D.E., & Semel, M. 1991, *A&A*, 250, 463
- Collier Cameron, A., 1992, in *Surface Inhomogeneities on Late-type Stars*, P.B. Byrne & D.J. Mullan, Berlin: Springer-Verlag, 33
- Donati, J.-F., & Collier Cameron, A., 1997, *MNRAS*, 291, 1
- Donati, J.-F., Semel, M., Carter, B., Rees, D.E., & Collier Cameron, A. 1997, *MNRAS*, 291, 658
- Donati, J.-F., Collier Cameron, A., Hussain, G.A.J., & Semel, M. 1999, *MNRAS*, 302, 477
- Guirado, J.C., et al. (22 authors) 1997, *ApJ*, 490, 835
- Hatzes, A.P. 1994, *ApJ*, 451, 784
- Hatzes, A.P., Vogt, S.S., Ramseyer, T.F., & Misch, A. 1996, *ApJ*, 469, 808
- Kürster, M. 1993, *A&A*, 274, 851
- Moore, C.E., Minnaert, M.G., & Houtgast, J. 1966, *The Solar Spectrum 2935 Å to 8770 Å* (NBS Monograph 61), Washington: National Bureau of Standards
- Piskunov, N.E., & Rice, J.B. 1993, *PASP*, 105, 1415
- Piskunov, N.E., & Wehlau, W.H. 1994, *A&A*, 289, 868
- Piskunov, N.E., Tuominen I., & Vilhu, O. 1990, *A&A*, 230, 363
- Press, W.H., Flannery, B.P., Teukolsky, S.A., & Vetterling, W.T., 1992, *Numerical Recipes: The Art of Scientific Computing* (2nd edition), Cambridge: Cambridge University Press
- Rice, J.B., & Strassmeier, K.G. 1996, *A&A*, 316, 164
- Rice, J.B., Wehlau, W.H., & Khokhlova, V.L. 1989, *A&A*, 208, 179
- Saar, S.H., Butler, R.P., & Marcy, G.W. 1998, *ApJ*, 498, L153
- Skilling, J., & Bryan, R.K. 1984, *MNRAS*, 211, 111
- Unruh, Y.C., & Collier Cameron, A. 1995, *MNRAS*, 273, 1
- Unruh, Y.C., & Collier Cameron, A. 1997, *MNRAS*, 290, L37

- Unruh, Y.C., Collier Cameron, A., & Guenther, E. 1998, MNRAS, 295, 781
Vogt, S.S., & Penrod, G.D. 1983, PASP, 95, 565
Vogt, S.S., Penrod, G.D., & Hatzes, A.P. 1987, ApJ, 321, 496